Delayed elasticity of metallic glasses: Loading time and temperature dependences of the anelastic relaxation

Mehran Nabahat [ORCID],[1] Narges Amini [ORCID],[2,3] Eloi Pineda [ORCID],[1,*] Fan Yang [ORCID],[3] Jichao Qiao [ORCID],[4] Beatrice Ruta [ORCID],[5] and Daniel Crespo [ORCID][1]

[1]*Department of Physics, Institute of Energy Technologies, Universitat Politècnica de Catalunya—BarcelonaTech, 08019 Barcelona, Spain*
[2]*Department of Chemistry, Aarhus University, 8000 Aarhus, Denmark*
[3]*Institut für Materialphysik im Weltraum, Deutsches Zentrum für Luft- und Raumfahrt (DLR), 51170 Köln, Germany*
[4]*School of Mechanics, Civil Engineering and Architecture, Northwestern Polytechnical University, Xi'an 710072, China*
[5]*Institut Lumière Matière, Université Claude Bernard—Lyon 1, CNRS, F-69622 Lyon, France*

One of the hallmarks of disordered matter is the large amplitude of the anelastic deformation, i.e., the fraction of reversible deformation that is not instantaneously recovered after the release of load but is delayed in time. In this paper, this delayed elasticity is studied for the glass-forming $Zr_{46.25}Ti_{8.25}Cu_{7.5}Ni_{10}Be_{27.5}$ alloy by means of stress step and recovery experiments. Even at high temperatures, not far from the glass transition, the delayed elasticity can recover an important fraction of the deformation and endure for a long time. Analyzing the effects of loading time and waiting time on the strain evolution, we reveal the presence of an anelastic response with a timescale dependent on loading time and an invariant shape, which indicates the presence of a distribution of reversible relaxation modes following a τ^{-n} law with exponent n between 0.5 and 1. The underlying distribution of energy barriers activated at different temperatures is accordingly shape invariant. Moreover, we found that a distribution of reversible modes corresponding to the high-frequency side of the α-relaxation peak can reproduce the experimental results. The results establish a direct link between the dynamical spectrum and the distribution of activation energies, revealing the origin of the transient creep and anelastic recovery behaviors of metallic glasses.

I. INTRODUCTION

How the atoms rearrange in amorphous materials is a fundamental question to understand their rheological and mechanical behaviors [1]. Disordered materials show complex relaxation dynamics at the molecular/atomic scale, involving various orders of magnitude in both time and length scales, as the mobility of the molecules (atoms in the case of metallic systems) is highly cooperative. Mechanical relaxation experiments, i.e., the application of small strains and stresses within the linear response regime, are a well-known tool to explore the dynamics of glasses [2]. In the case of metallic glasses (MGs), whose conductive nature impedes electric relaxation experiments, mechanical tests become a unique tool to obtain direct information of the atomic movements.

Above the glass transition, in the supercooled liquid (SCL) state, the relaxation dynamics of many disordered substances can be characterized by a stretched relaxation modulus described by a Kohlrausch-Williams-Watts (KWW) function. Recent studies on $Zr_{46.25}Ti_{8.25}Cu_{7.5}Ni_{10}Be_{27.5}$ (Vit4) alloy have shown that, in the SCL, the relaxation time, obtained from stress relaxation and oscillation strain measurements, follows a Vogel-Fulcher-Tammann (VFT) temperature behavior in accordance with viscosity measurements and with the microscopic dynamics at the length scale of atomic-atomic distances as probed by x-ray photon correlation spectroscopy (XPCS) [3]. An important aspect is that the viscous liquid material above the glass transition temperature T_g shows an invariant relaxation shape, with a KWW exponent between 0.5 and 0.6, indicating the validity of time-temperature superposition in this region and the participation of a broad relaxation time distribution in the process [3–5].

The relaxation of MGs becomes more complex in the glass transition region. At these temperatures, due to the super Arrhenius increase of the structural relaxation time, the system cannot reach the SCL equilibrium configuration within the laboratory timescale. Therefore, the study of the relaxation dynamics is always affected by physical aging, and it becomes challenging due to the long timescales involved in both mechanical relaxation and physical aging [6]. Previous stress relaxation experiments in MGs show a progressive stretching of the relaxation modulus as the system is driven out of equilibrium, indicating a broadening of the relaxation time distribution in the glass state [3,5,7]. One important feature to understand glass dynamics is the contribution of anelastic relaxations [8,9], which may have a different temperature sensitivity than the viscous process governing the relaxation in the liquid. In most experimental studies, the coincidence of timescale between anelasticity (or delayed elasticity), the permanent structural rearrangements due to physical aging, and the permanent plastic deformation makes it difficult to disentangle each contribution and obscures the interpretation of the results.

* eloi.pineda@upc.edu

The aim of this paper is to focus on the anelastic relaxation of MGs, unveiling its main features and providing a clear picture considering the current models and theoretical frameworks of MG dynamics. With this purpose, we study the creep and recovery behavior, i.e., the response under stress step experiments, of the Vit4 MG. We restrict the study to small stresses and deformations, always within the linear regime, and a range of temperatures from 0.83 T_g up to near T_g. In the following sections, we will detail the experimental methods and we will show how the recovery relaxation function depends on loading time and temperature. We will show that the intensity distribution of anelastic modes has an invariant shape over a broad range of times and temperatures. This produces an anelastic recovery with an amplitude that increases with temperature and a timescale that is only dependent on the previous loading time. Finally, we will analyze the shape of the distribution of anelastic modes and discuss its relationship with the mechanical relaxation spectrum in the frequency domain.

II. MATERIALS AND METHODS

Creep and recovery experiments of Vit4 ribbons were performed in tensile geometry in a DMA Q800 apparatus (see Fig. S0 in the Supplemental Material [10]). The constant stresses applied during the creep segment went from 20 to 400 MPa. The strain recovery after the creep was followed while applying a small force of 0.01 N (<0.2 MPa) to maintain the straight shape of the ribbon pieces. The experiments were carried isothermally at temperatures from 520 to 580 K. Before the creep-recovery experiments, the ribbons were annealed for 60 min at 590 K, just below the onset of the glass transition, to relax as-quenched stresses and ensure a similar, initial structural state for all the samples. Different lengths of the creep and recovery segments have been applied in this paper. Preliminary tests applying creep times of 10 h and recovery times of 20 h were performed to better determine the end of the recovery process (see Figs. S1 and S2 in the Supplemental Material [10]). The standard experiments were carried out by applying 10 h of creep and 10 h of recovery to optimize the experimental time. Preliminary tests, with longer recovery steps, were used to estimate the final strain value at the end of the recovery. Additionally, experiments with different creep times from 200 to 800 min were also done, always maintaining a recovery time that was longer than the creep time.

Complementary stress relaxation and mechanical spectroscopy experiments were already performed on Vit4 ribbons [3]. Stress relaxation was measured, applying a constant deformation step of $\varepsilon = 0.1\%$ and monitoring how the stress decays with time. The mechanical spectroscopy measurements were performed at a heating rate of 1 K/min with driving frequencies from 0.03 to 30 Hz. The results of stress relaxation at different temperatures in the glass and SCL states

and the loss modulus obtained from mechanical spectroscopy were already shown and discussed in Ref. [3]. Here, some additional tests were performed to complement the information on how stress relaxation evolves with aging in the glass state.

III. RESULTS: PHENOMENOLOGICAL FEATURES OF THE CREEP-RECOVERY BEHAVIOR

The glass transition of Vit4 is observed at $T_{g,10} = 622$ K when heating at a rate of 10 K min^{-1}. The glass transition at a heating rate of 0.1 K min^{-1} can be estimated to be at $T_{g,0.1} = 592$ K [11]. Therefore, for isothermal tests, we can consider that the system is very close to the equilibrium SCL configuration >590 K. The range of temperatures studied in this paper goes from $T = 0.83 T_{g,10}$ to $0.95 T_{g,10}$, in which MGs show homogeneous plastic deformation under the strain rates that are usually tested in mechanical experiments and applied in some processing technologies like thermoplastic forming [12]. Figure 1 shows the strain of a Vit4 sample during a tensile creep-recovery test at 580 K. In this case, the curve consists of two consecutive creep-recovery cycles, with creep and recovery segments of 600 min each. The different magnitudes observed in Fig. 1 are defined as the following: ε_{ec} and ε_{er} are the elastic jump and drop at the loading and unloading instants; ε_{pl} is the final permanent deformation after the creep-recovery cycle; $\varepsilon_{ac}(t)$ is the retardation function during the transient creep stage, calculated subtracting the contribution of the viscous deformation $\dot{\varepsilon} = \sigma/\eta$. The apparent extensional viscosity value η is calculated from the slope $\dot{\varepsilon}$ at the end of the creep segment; $\varepsilon_{ar}(t)$ is the relaxation of strain during the recovery, calculated subtracting the final ε_{pl}. The $\varepsilon_{ac}(t)$ and $\varepsilon_{ar}(t)$ functions are the difference between experimental data (symbols) and the dashed lines in Fig. 1. A notable characteristic of the creep-recovery curves shown in Fig. 1 is that the creep segment of the first cycle shows a clear higher amplitude than in the second cycle, while the recovery segments are essentially equal. This feature is well known in creep tests of MGs since the work of Maddin and Masumoto [13], and it will be further discussed below. It must be noted that the apparent viscosity η, used to plot the dashed lines in the creep segments of Fig. 1 and to calculate $\varepsilon_{ac}(t)$, is a lower bound value of the steady-state viscosity. Longer creep segments would be necessary to estimate the steady-state, isoconfigurational viscosity [8]. The implications of this point will also be discussed in the following section.

One important aspect of mechanical tests is to check if the experiment is performed in the linear response region. In this paper, all the curves up to $\sigma = 200$ MPa were found completely linear with stress at all temperatures (see Fig. S3 in the Supplemental Material [10]). Only >350 MPa at 580 K is the onset of the nonlinear response observed, characterized by a non-Newtonian viscosity behavior [14]. Therefore, unless otherwise stated, all the results shown in this paper will be considered in the linear region. This allows us to describe the creep-recovery curves as

$$J(t) = \frac{\varepsilon(t)}{\sigma} = \begin{cases} E^{-1} + J_{ac0}[1 - \phi_{ac}(t)] + \frac{t}{\eta}, & \text{for } t \leqslant t^*, \\ J(t^*) - E^{-1} + J_{ar0}\phi_{ar}(t'), & \text{for } t' = t - t^* > 0, \end{cases} \qquad (1)$$
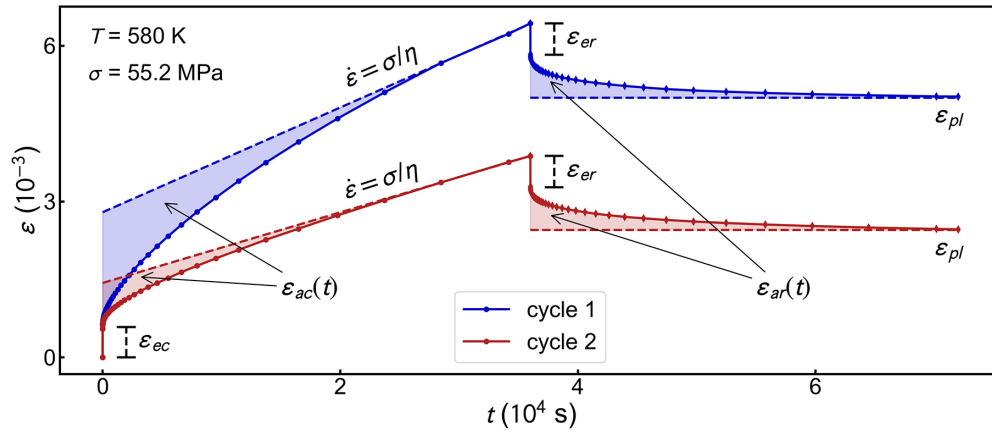
FIG. 1. Evolution of strain during two consecutive creep-recovery cycles at 580 K. Each creep and recovery segment lasted 600 min, the whole duration of a cycle being 1200 min. To better compare the two curves, the strain and time axes of the second cycle are shifted by setting $\varepsilon = t = 0$ at the end of the first cycle.

where t^* is the time at the end of the creep segment, E is the elastic modulus, η is the extensional viscosity, $J_{ac0} = \frac{\varepsilon_{ac}(t=0)}{\sigma}$ and $J_{ar0} = \frac{\varepsilon_{ar}(t'=0)}{\sigma}$ are the transient creep and recovery amplitudes, and finally, $\phi_{ac}(t) = \frac{\varepsilon_{ac}(t)}{\varepsilon_{ac}(0)}$ and $\phi_{ar}(t') = \frac{\varepsilon_{ar}(t')}{\varepsilon_{ar}(0)}$ are the creep-retardation and recovery-relaxation functions going from 1 to 0 as time elapses. Figures 2(a) and 2(b) shows the invariant shapes of $\phi_{ac}(t)$ and $\phi_{ar}(t)$ found

for different values of applied stress at 580 K, further validating the linear response behavior of the whole creep-recovery curve. For the experiments shown in Fig. 2, all the creep segments had a duration of $t^* = 600$ min, independently of the stress and temperature applied, and they correspond to the results of a single creep and recovery cycle.
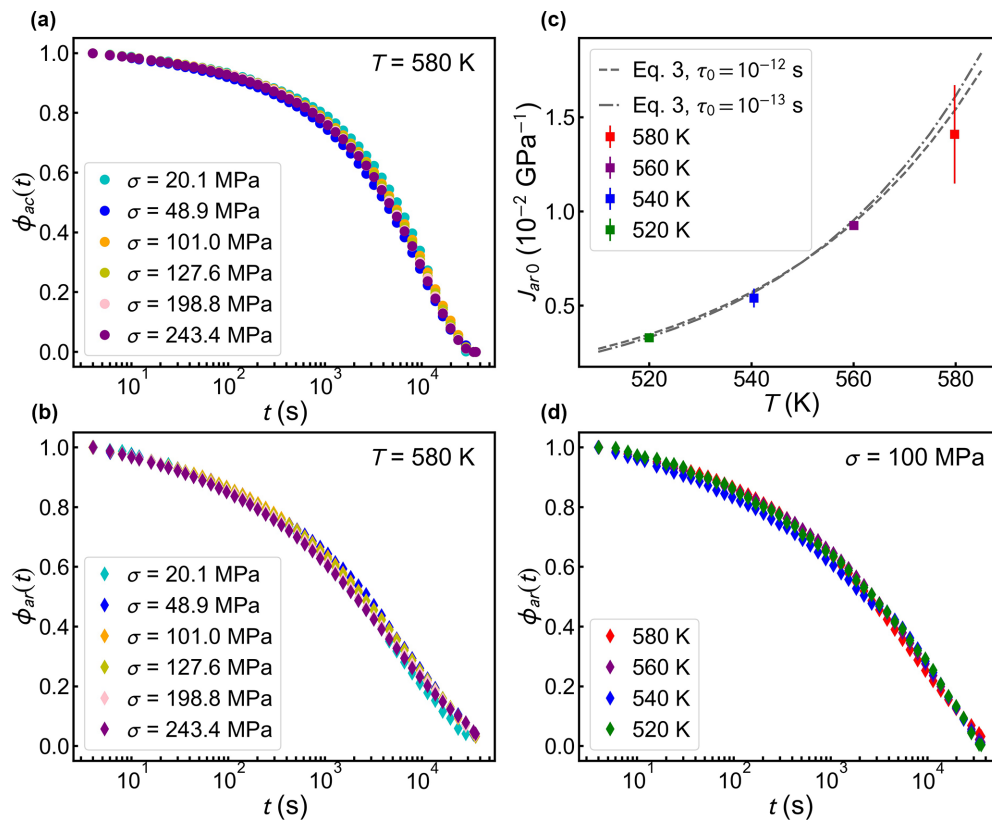

FIG. 2. (a) Creep-retardation $\phi_{ac}(t) = \varepsilon_{ac}(t)/\varepsilon_{ac}(0)$ and (b) recovery-relaxation $\phi_{ar}(t) = \varepsilon_{ar}(t)/\varepsilon_{ar}(0)$ functions obtained at 580 K for the first cycle of creep-recovery tests with different applied stresses. (c) Amplitude of the recovery relaxation and (d) recovery-relaxation functions at 520, 540, 560 and 580 K. All tests were performed with a creep duration of $t^* = 600$ min. The dashed line in (c) is the prediction of change of anelastic amplitude calculated by means of Eq. (3).
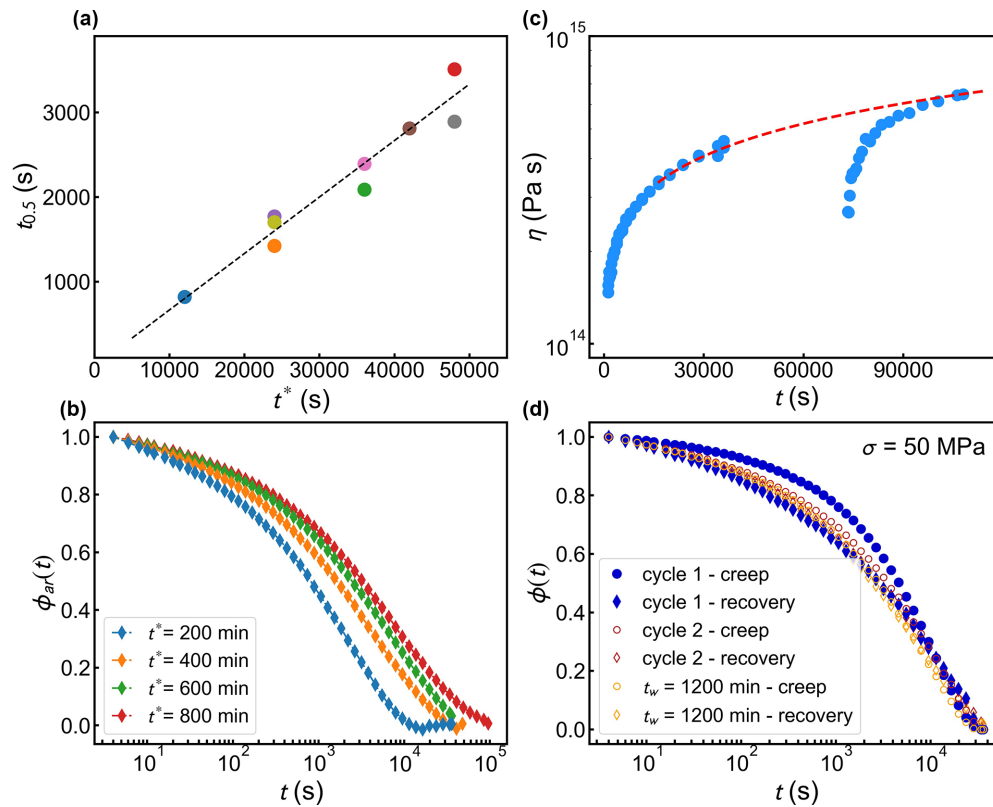
FIG. 3. (a) Time to reach half recovery after creep segments of duration t^*. (b) Recovery-relaxation functions after creep segments of duration t^*. (c) Apparent extensional viscosity $\eta = \sigma/\dot{\varepsilon}$ calculated at different times during creep segments initiated at two different waiting times. (d) Creep-retardation and recovery-relaxation functions for two consecutive creep-recovery cycles and a cycle initiated after a waiting time of 1200 min. All tests in this figure were performed at 580 K.

The amplitudes of creep retardation and recovery relaxation are sensitive to temperature. Figure S4 in the Supplemental Material [10] shows creep-recovery curves measured at different temperatures. Figures 2(c) and 2(d) show, respectively, the recovery amplitude and the recovery relaxation function for the four temperatures studied in this paper. It can be observed that the amplitude of the relaxation increases with temperature, but the relaxation function is completely invariant. Therefore, a notable aspect of the recovery relaxation function is that its shape and timescale are not dependent on temperature or stress, which is a first important property we would like to highlight in this paper.

Conversely, the timescale of the relaxation function depends on the duration of the previous external excitation. Figure 3(a) shows the timescale of the recovery relaxation, estimated as the time $t_{0.5}$ needed to decay to $\phi_{\mathrm{ar}}(t) = 0.5$, as a function of the duration of the previous creep segment t^*, all measurements performed at 580 K. Figure 3(b) shows the recovery relaxation functions measured after step stress segments of different duration, showing the progressive shift to longer times as a function of t^*. Changes of temperature and stress do not modify the time needed for recovery, as the normalized $\phi_{\mathrm{ar}}(t)$ function is invariant with respect to such parameters. As it is shown in Fig. 3(a), the duration of the recovery relaxation is basically proportional to the time the system has been under the application of external stress in the previous creep stage. This is a second basic characteristic of the recovery process. The implications of this behavior,

together with the athermal character of the relaxation shape noted above, will be discussed in the following section.

As already noted above in Fig. 1, the amplitude of the creep process during a first cycle is notably higher than in a posterior cycle. To check if such a change is because of the applied stress or because of physical aging driven by the isothermal annealing, we performed a first cycle of creep-recovery after annealing for 1200 min at 580 K (see Fig. S5 in the Supplemental Material [10]). As it is observed in Fig. S5 in the Supplemental Material [10], the reduction of the creep amplitude in a second cycle is like the one found in a first cycle after annealing, under the condition that the duration of the previous isothermal annealing is the same as that of the test cycle. Therefore, the change in the creep segment between the first and posterior cycles can be mainly attributed to physical aging, which drives the glass toward a more stable, denser, and sluggish configuration. Figure 3(c) shows the change of the apparent extensional viscosity, calculated as $\eta'(t) = \sigma/\dot{\varepsilon}(t)$, along two creep segments: one initiated at the beginning of the isothermal step and the other after a waiting time of 1200 min. Two main aspects can be observed. Firstly, a constant viscosity is not reached after 600 min at 580 K. This means that the extensional viscosity values obtained by $\eta = \sigma/\dot{\varepsilon}(t^*)$ at the end of the creep segment are just an approximation to the steady-state extensional viscosity. Secondly, there is a clear effect of aging on the extensional viscosity, which is not finished even after 30 h. Below T_g, the equilibrium viscosity is far above the viscosity of the glass, and aging increases

viscosity [15] at a rate that can be dependent on composition and temperature [16]. In the time window explored in this paper, the extensional viscosity at 580 K is found to follow approximately an aging law given by $\eta \propto t^{0.5}$. The equilibration timescale of the extensional viscosity, of the order of 10^4–10^5 s, is like the one found for shear viscosity in the same material at similar temperatures [11]. Figure 3(d) shows the creep-retardation and recovery-relaxation functions, $\phi_{\mathrm{ac}}(t)$ and $\phi_{\mathrm{ar}}(t)$ calculated for the first cycle, second cycle, and first cycle after a waiting time of 1200 min, i.e., the same amount of time employed for the first cycle. While the creep-retardation function during the first cycle shows a clearly different shape, all the other functions mainly overlap. This implies that, when the effects of physical aging on viscosity are diminished, i.e., the rate of change of viscosity along the creep experiment is small, we found $\phi_{\mathrm{ac}}(t) \approx \phi_{\mathrm{ar}}(t)$. Figure S6 in the Supplemental Material [10] shows the $\phi_{\mathrm{ac}}(t)$ functions obtained at different temperatures. In accordance with the expected increase in aging rate as temperature rises, it has been observed that the effect of aging on the shape of the retardation function increases with temperature. On the contrary, as already depicted in Fig. 2(d), the recovery functions are temperature invariant.

The results shown in Figs. S5 and S6 in the Supplemental Material [10] and Figs. 3(c) and 3(d) evidence two important facts. Firstly, a stress-oriented structural relaxation effect, as found by Khonik *et al.* [17], is not observed. It is possible that part of the directional effect described in Ref. [17] is erased during the recovery step before the second creep-recovery cycle. It is also possible that different MG compositions may show different influence of stress on structural relaxation. In our case, we do not observe differences in deformation behavior between aging under stress and aging without stress. Secondly, the transient stage of the creep curve contains the contribution of a time-dependent viscosity. This implies that the amount of permanent deformation does not increase linearly as $\frac{t}{\eta}\sigma$ because $\eta = \eta(t)$ due to aging. However, if the aging rate is slower than the timescale involved during the relaxation, as it is in the case of the creep curves measured after annealing 1200 min at 580 K, the permanent deformation can be approached to a linear term with time, and then the transient stage of the creep is mainly contributed only by the anelastic retardation. In other words, the coincidence of retardation and relaxation functions, i.e., $\phi_{\mathrm{ac}}(t) \approx \phi_{\mathrm{ar}}(t)$, implies that, for the aged samples, the transient stage of creep is mainly contributed by reversible deformation. This is clearly shown in Fig. 1, where $\varepsilon_{\mathrm{ac}}(t)$ and $\varepsilon_{\mathrm{ar}}(t)$, indicated by the colored regions, are equal for cycle 2.

IV. DISCUSSION: TIMESCALE AND SHAPE OF THE ANELASTIC RESPONSE

Most of the theoretical descriptions of liquids predict that, below a certain dynamic transition, the relaxation becomes dominated by thermally activated mechanisms, while collisional transport is expected above [18]. These activated mechanisms become more cooperative as temperature decreases. Going down on temperature, toward the glass transition, the increase of the apparent activation energy for flow can be related to the number of atoms involved in the coopera-

tive relaxation events [19] and to the shape of the cooperative rearrangement regions [20]. Below T_g, the deformation of MGs is generally interpreted in terms of soft spots or shear transformation zones (STZs). Both the size and number density of such soft spots is expected to decrease with aging [21]. In the steady state, plastic deformation of MGs under a constant strain rate is usually described by the thermally activated operation of STZs and diffusive jumps in regions of high free volume [22–24]. The creep curves are then usually interpreted considering an initial, transient stage of nucleation and distribution of local strain. This process progressively approaches saturation, leading to a secondary, steady-state stage with constant strain rate. A tertiary stage characterized by the onset of structural instability is observed if the creep is maintained up to large strain values, which is not the case in this paper.

The creep (stress step) and recovery results presented above, together with the stress relaxation (strain step) and mechanical spectroscopy (oscillating strain) measurements already discussed in Ref. [3], point toward the following picture of Vit4 glass dynamics. The mobility of the atoms generates two different contributions: a reversible anelastic or delayed elasticity behavior and a permanent, irreversible viscouslike relaxation. The latter process generates a steady-state Newtonian viscosity $\eta(T_f, T)$ and a corresponding stress relaxation time $\tau_{\mathrm{sr}}(T_f, T)$ that dictate the timescale of the irreversible relaxation and depend on the fictive temperature T_f of the glass structure. The homogeneous viscous flow of MGs has been well studied, and it can be well understood in terms of the free volume model [23,25–27]. The viscous flow is a thermally activated process which is biased by the application of stress. As it is observed in many MGs at temperatures comparable with the one investigated in this paper, an increase in stress produces a change from Newtonian to non-Newtonian flow >200–400 MPa [28]. In the linear response regime, at small stresses, the viscosity shows a super-Arrhenius (VFT) behavior above T_g and an Arrhenius-like behavior for a given isoconfigurational glass state [29]. In practice, aging is always present in the glass state, and a time-dependent viscosity $\eta[T_f(t), T]$ must be expected in isothermal experiments exploring long timescales.

In addition to the viscous irreversible deformation, Vit4 shows a large anelastic response. Figure 1 shows that, for $t^* = 600$ min at 580 K, the fraction of deformation that is recovered anelastically is larger than the elastic contribution. Applying the same loading time t^* at different temperatures, the amplitude of the anelastic response is reduced as temperature decreases, but the anelastic recovery for $t^* = 600$ min at 520 K is still 30% of the elastic deformation (see Fig. S4 in the Supplemental Material [10]). This temperature is 100 K below the conventional glass transition, as measured by calorimetry with a heating rate of 20 K/min. The control of the anelastic deformation and the corresponding recovery are then important aspects to consider for controlling the mechanical response of MGs in many applications. Such significant delayed elasticity behavior is a known effect in MGs [30], but it is still little understood and will be discussed here in detail.

Firstly, it is worth noting again that, in an isoconfigurational glass, the viscosity would be constant at a given temperature, but in the real aging glass, it increases during
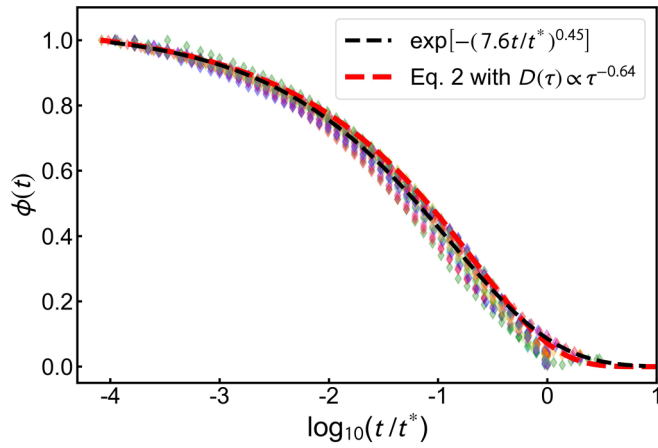
FIG. 4. Symbols: Master curve of the recovery functions obtained in this paper for different values of stress ($\sigma = 20-400$ MPa), temperature ($T = 520-580$ K), loading time ($t^* = 200-800$ min at 580 K) and aging time (3.2–30 h at 580 K). A total number of 30 recovery functions corresponding to different conditions are plotted. Black dashed line: Kohlrausch-Williams-Watts (KWW) function with stretching parameter $\beta = 0.45$. Red dashed line: Recovery-relaxation function calculated by Eq. (2) considering $D(\tau) \propto \tau^{-0.64}$ and $t^* = 1$.

the creep test at a rate depending on temperature and the T_f of the initial state [6]. As seen in Fig. 3(d), this is reflected in the creep tests, producing a different shape of the retardation function with respect to the recovery function for the samples that were not deeply aged previously. If viscosity η is not constant, it is difficult to disentangle the pure anelastic response and the shape of the retardation function from the creep segment by using Eq. (1). On the other hand, the recovery segment in Eq. (1) is not affected by a time dependent viscosity, and therefore, it gives access to a better description of the anelastic response [31,32]. From this point on, we will use the notation $\phi(t)$ for the recovery functions, as we will focus on them.

Figure 2(d) shows that the recovery relaxation function $\phi(t)$ is invariant with temperature. The loading time effect on the recovery, shown in Figs. 3(a) and 3(b), indicates that the timescale increases with t^*. Figure 4 shows all the recovery functions $\phi(t)$ experimentally obtained for different temperatures and different loading times as a function of t/t^*. They can be well described by a master curve following a stretched exponential $\phi(t) = \exp[-(\Gamma t)^\beta]$, with a shape parameter $\beta = 0.45$ and $\Gamma = 7.6/t^*$ (black dashed line).

The loading time effect observed in Figs. 3(a), 3(b), and 5 implies that the anelastic response can be interpreted as the excitation/relaxation of reversible modes [33,34], each mode defined by a characteristic time τ. These modes are progressively excited, i.e., strained, during the loading segment t^*, and they relax back to the original state during the recovery. In a first approach, the recovery can be modeled as

$$\phi(t) = A^{-1} \int_0^\infty d\tau D(\tau)\Theta(t^* - \tau)\exp\left(-\frac{t}{\tau}\right)$$
$$= A^{-1} \int_0^{t^*} d\tau D(\tau)\exp\left(-\frac{t}{\tau}\right), \quad (2)$$

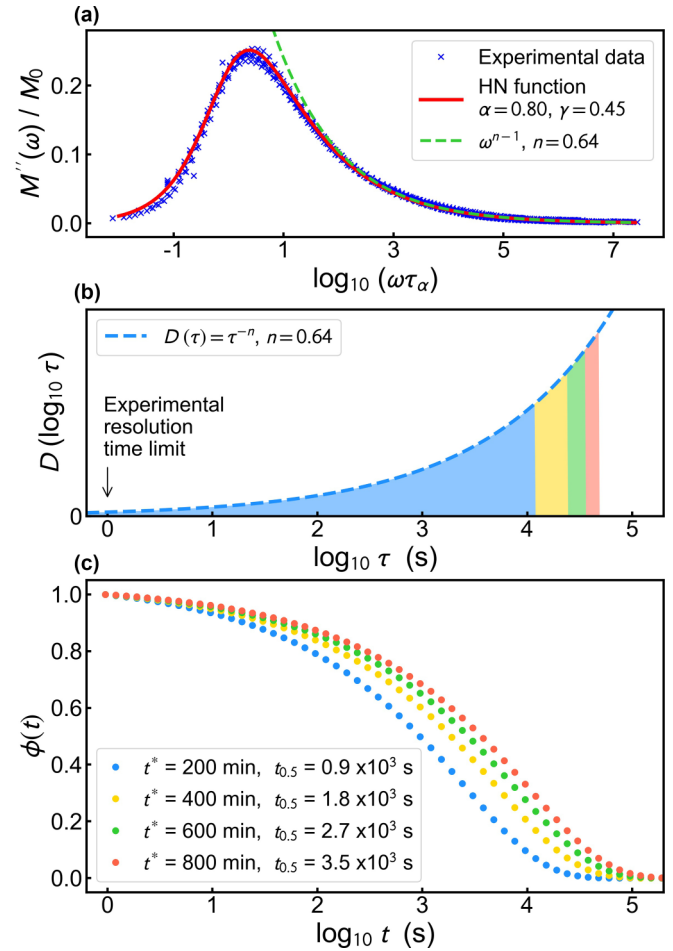FIG. 5. (a) Master curve of the loss modulus of Vit4 glass as a function of $\omega\tau_\alpha$, where τ_α is the α relaxation time. See Ref. [3] for details. (b) Distribution of relaxation modes (blue dashed line) considering a distribution of reversible modes $D(\tau) \sim \tau^{-0.64}$ (dashed line). The excited modes after loading during $t^* = 200, 400, 600,$ and 800 min are shown by the blue, yellow, green, and red areas, respectively. (c) Recovery functions calculated by Eq. (2) with $D(\tau) \sim \tau^{-0.64}$. The legend also shows the calculated times needed to reach half recovery after different excitation times t^*, which are in good agreement with the experimental results in Fig. 3(a).

where $D(\tau)$ is the intensity distribution of modes τ, $\Theta(x)$ is the Heaviside step function, and $A = \int_0^{t^*} d\tau D(\tau)$ is the normalization needed for $\phi(t)$ going from 1 to 0. Each mode is considered to behave linearly, i.e., with an exponential relaxation $\propto \exp(-t/\tau)$. This assumption of linearity is appropriate if small stress and strain conditions are assumed [33], as it is the case in this paper. Equation (2) assumes that all the modes with $\tau < t^*$ are excited during the loading segment. The longer the t^*, the more modes become excited, and their relaxation is then observed in the recovery. The stretched shape of the $\phi(t)$ function, seen in Fig. 5, is indicative of a broad distribution $D(\tau)$. A distribution of the type $D(\tau) \propto \tau^{-n}$, with $0.5 < n < 1$, can reproduce similar results to the ones observed experimentally, as it was already shown by Ulfert and Kronmüller [9] in their study of the creep-recovery curves. Figure S7 in the Supplemental Material [10] shows the fraction of excited modes for different loading times

t^*, as well as the corresponding calculations of the recovery function using Eq. (2), for values of $n = 0.5$, 0.75, and 1. The insets in Fig. S7 in the Supplemental Material [10] also show the timescale $t_{0.5}$ of the calculated recovery functions. The limiting cases of $n = 1$, i.e., a completely flat distribution in the logarithmic scale, and $n = 0.5$ produce too short and too long timescales, respectively. In the case of $n = 1$, the recovery is too fast because of the presence of a too large fraction of fast modes excited during the loading. Conversely, a distribution shape determined by $n = 0.5$ contains a too small fraction of fast modes. A middle value $n \sim 0.75$ reproduces qualitatively the timescale shown in Fig. 3(a).

Information of the relaxation spectrum is given by the complex modulus $M^*(\omega) = M'(\omega) + iM''(\omega)$ obtained by mechanical spectroscopy. In the case of Vit4, the loss modulus $M''(\omega)$ shows a broad α relaxation peak with a long high-frequency wing, as shown in Fig. 5(a), and it can be perfectly described by a Havriliak-Negami function $M^*(\omega) = [1 + i(\omega\tau)^\alpha]^{-\gamma}$ [35] with shape exponents $\alpha = 0.80$ and $\gamma = 0.45$. The high-frequency wing of the loss modulus decays as ω^{-a} with $a \approx \alpha\gamma = 0.36$ [36]. We will make the ansatz here that the high-frequency range of the mechanical spectrum contains basically the reversible relaxation modes generating the anelastic response. From a simple analysis (see Sec. 7 in the Supplemental Material [10]), it can be shown that a distribution of the type $D(\tau) \propto \tau^{-n}$ generates a high-frequency wing decaying as ω^{n-1}. Therefore, the experimental $M''(\omega)$ suggests a value of $n \sim 0.64$ for the distribution of reversible relaxation modes in the Vit4 material. Figure 5(b) shows this distribution of modes, mimicking the mechanical spectrum, and the fraction of them excited during different loading times t^*. Figure 5(c) shows the calculated recovery functions using Eq. (2) and the corresponding $t_{0.5}$ times needed to reach half recovery. The timescales of the recovery are in perfect agreement with the experimental observations in Fig. 3(a). The shape of the recovery functions is also plotted with a red dashed line in Fig. 4, showing excellent agreement with the experimental results.

Now we will explore the effects of temperature on the anelastic recovery. In their formidable study, Argon and Kuo [30] demonstrated that the recovery of MGs is thermally activated, as it can be frozen by immediate quenching after a creep experiment and posteriorly activated by subsequent heating. Each relaxation mode was then associated to an activation energy $\tau = \tau_0 \exp(E/kT)$, with τ_0^{-1} of the order of the Debye frequency, and they determined experimentally the distribution of activation energies by a series of creep-quenching-heating-recovery cycles. The shape of the distribution $D(E)$ they found for different materials was qualitatively like the shape shown in Fig. 5 for $D(\log_{10}\tau)$, i.e., an increasing function with a maximum around $E^* \approx kT \ln(t^*/\tau_0)$, which corresponds to the activation energy of the longest excited modes during the previous loading segment. Also in Ref. [37], the time distribution of the anelastic recovery $D(\log_{10}\tau)$, obtained from nanoindentation tests, was found to be an increasing function with a cutoff around t^*. Here, we have shown in Figs. 2(d) and 4 that the recovery relaxation function has an invariant shape at different temperatures and loading times, at least within the experimental time window which in this paper covers from 1 to 10^5 s. This also implies

that the underlying distribution of activation energies of the Vit4 glass has an invariant normalized shape with a maximum value E^* determined by temperature and loading time.

Considering that each anelastic mode is associated to an activation energy, the fraction of modes excited after a loading time t_1^* at a temperature T_1 must be the same as after time t_2^* at T_2 if $T_1 \ln(t_1^*/\tau_0) = T_2 \ln(t_2^*/\tau_0)$. Therefore, the temperature dependence of the amplitude of the anelastic recovery $J_{\mathrm{ar0}}(T)$ for a given loading time t^* can be calculated as

$$\frac{J_{\mathrm{ar0}(T,t^*)}}{J_{\mathrm{ar0}}(T_{\mathrm{ref}}, t^*)} = \frac{\int_{t'_{\mathrm{min}}}^{t^{*\prime}} d\tau D(\tau)}{\int_{t_{\mathrm{min}}}^{t^*} d\tau D(\tau)}, \tag{3}$$

where t_{min} is the time resolution of the experiment, $T \ln(t^{*\prime}/\tau_0) = T_{\mathrm{ref}} \ln(t^*/\tau_0)$, and $T \ln(t'_{\mathrm{min}}/\tau_0) = T_{\mathrm{ref}} \ln(t_{\mathrm{min}}/\tau_0)$. Considering a distribution $D(\tau) \propto \tau^{-n}$, Eq. (3) gives $(t^{*\prime 1-n} - t'^{1-n}_{\mathrm{min}})/(t^{*1-n} - t^{1-n}_{\mathrm{min}}) \sim (t^{*\prime}/t^*)^{1-n}$, which allows us to calculate the relative change of the amplitude of anelastic recovery at different temperatures. Figure 2(c) shows with a dashed line the calculation of $J_{\mathrm{ar0}}(T, t^*)$, taking $n = 0.64$, $T_{\mathrm{ref}} = 550$ K, $t_{\mathrm{min}} = 1$ s, and $t^* = 600$ min; the latter two are the time resolution and duration of the creep tests shown in Fig. 2. Two values of τ_0, 10^{-12} and 10^{-13} s, were considered to check that the calculation is not significantly affected by this parameter. These values of τ_0 are like the ones found in Ref. [30] and of the order of the inverse of the Debye frequency. It can be seen in Fig. 2(c) that the change of anelastic amplitude with temperature given by Eq. (3) is in good agreement with the experimental data. Figure S8 in the Supplemental Material [10] further illustrates the fraction of activation energies excited during the same loading time t^* at different temperatures, as well as the corresponding recovery functions. In terms of the amplitude of anelastic recovery, a loading time of $t^* = 600$ min at 510 K is equivalent to loading during $t^{*\prime} = 32$ min at 550 K. In the opposite direction, a loading time $t^* = 600$ min at 570 K is equivalent to $t^{*\prime} = 2610$ min at 550 K. Therefore, the temporal scale, the functional shape, and the temperature dependence of the experimental data can all be replicated by a distribution $D(\tau) \propto \tau^{-n}$ of reversible modes with $n = 0.64$, which is coincident with the shape of the high-frequency tail of the α-relaxation peak.

We have tried different values of n and alternative ways to compute the fraction of reversible modes excited during the loading segment. For instance, we performed all the calculations supposing that the intensity of activated modes was $D(\tau)[1 - \exp(-t^*/\tau)]$, instead of $D(\tau)\Theta(t^* - \tau)$, which is a logical assumption considering a linear behavior [33]. With this approach, the cutoff at t^* is too smooth to reproduce the shape and timescale of the experimental recovery functions. Inspection of Fig. 4 shows that the recovery always finishes very close to t^*. Therefore, an abrupt cutoff of the excited modes at t^* seems necessary to reproduce quantitatively all the experimental facts. In this paper, we have modeled the cutoff by a step function $\Theta(t^* - \tau)$, but similar results would be obtained for any cutoff function able to restrict the participation of relaxation modes up to timescales of the same order than t^*. It is also worth noting that, in all the calculations, only the anelastic modes with τ longer than the experimental resolution, $t_{\mathrm{min}} \sim 1$ s in this paper, are considered. Below
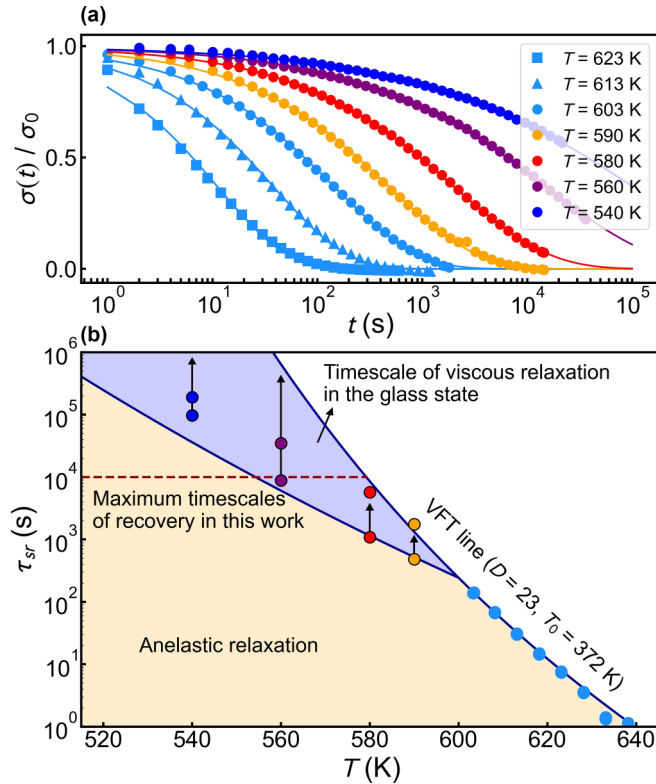
FIG. 6. (a) Examples of Vit4 stress relaxation curves obtained at different temperatures. (b) Vit4 stress relaxation times at the supercooled liquid (SCL) state (light blue circles) and at the glass state (orange, red, purple, and blue circles). In the glass state, two relaxation times are displayed for each temperature corresponding to the as-quenched state and the most aged sample. The arrows indicate the increase of relaxation time as a function of aging in the glass state. The blueish area in the time-temperature map corresponds to the timescales expected for the viscous relaxation, which depend on the aging state. The higher border of the blueish area is the extrapolated equilibrium Vogel-Fulcher-Tammann (VFT) line $\tau_{sr} = \tau_0 \exp(\frac{DT_0}{T - T_0})$ with $D = 22.7$ and $T_0 = 372$ K, and the lower border is an Arrhenius line with fictive temperature $T_f = 600$ K and activation energy $E = 270$ kJ mol^{-1}.

this limit, the relaxation of faster modes is detected by the equipment as part of the instantaneous elastic response and cannot be explored experimentally.

In the opposite direction, toward long times, the experiments performed at 580 K reach timescales like the ones of the viscous process. Beyond this viscous limit, the stress must be irreversibly relaxed, thus determining the long-time limit of the anelastic memory. Figure 6 shows the stress relaxation curves and their characteristic times τ_{sr}, measured both in the SCL state and in the glass state by means of stress relaxation (strain step) experiments. In such tests, once the stress decays to zero, the applied deformation becomes permanent, indicating the timescale $\tau_{sr}(T_f, T)$ of the irreversible viscous process. These stress relaxation times are in accordance with the α relaxation times obtained by mechanical spectroscopy, as discussed in Ref. [3]. As seen in Fig. 6(b), in the SCL state, the relaxation times can be described by a VFT behavior in accordance with the equilibrium viscosity of Vit4

[3]. Otherwise, in the glass state <600 K, the relaxation time changes with aging. Figure 6(b) shows two different τ_{sr} values for each temperature in the glass state: one obtained for as-quenched samples and another after a waiting time of ~40 h at each temperature. The blueish area in Fig. 6(b) is meant to indicate the broad time-temperature region where the viscous relaxation can be found for different glass states with different degrees of aging. The yellowish area indicates the timescales covered by the reversible anelastic relaxation, which expands from times shorter than the resolution limit in this paper (1 s) to the timescale of the irreversible viscous process. The effect of aging on atomic mobility and stress relaxation in Vit4 will be discussed in future work. Here, we just want to give an overall picture of the timescale expected for the irreversible relaxation at different temperatures, while we focus on the study of the reversible, anelastic contribution.

The effect of the viscous cutoff on the anelastic response would be to deplete the reversible modes with τ few times longer than τ_{sr}. Therefore, it is expected to affect the tail of the longest recovery functions at temperatures near the glass transition. This may be the reason why the amplitude of the anelastic recovery calculated by Eq. (3) seems to slightly overestimate the experimental value at 580 K, as seen in Fig. 2(c). A series of further experiments, pushing the experimental times at both the short and long limits, would be interesting to check the range of validity of the results presented here.

In the last part of this section, we will summarize the main results of this paper and discuss the observed behavior within the frame of previous results and current microscopic models of MG deformation. From the results presented above, the transient creep and the recovery behaviors of Vit4 can be described by the presence of a distribution of anelastic relaxation modes, each relaxation mode associated to an activation energy $E \approx kT \ln(\tau/\tau_0)$. The main result of this paper is that the distribution of times, and therefore of activation energies, shows an invariant normalized shape over different temperatures and loading times. In addition, the shape of the distribution can be related to the high-frequency wing of the mechanical spectrum $M''(\omega)$. MGs are characterized by a broad $M''(\omega)$ peak [38], extending over many decades in frequency, and this explains the large delayed elasticity effect in these materials.

It is worth commenting here that Vit4 does not show a significant secondary relaxation in its mechanical spectrum. In other MGs, with prominent secondary relaxations, the effect on the anelastic modes distribution may be important. For instance, it is well known that aging significantly alters the intensity of the secondary process [38]. In fact, Castellero *et al.* [37] and Lei *et al.* [32] found that, in other systems with more prominent secondary relaxation, aging altered the shape of the underlying distribution of activation energies. The simple shape of the anelastic mode distribution found here for different temperatures and different degrees of aging may be related to the particularly stable structure of the Vit4 glass. The characterization of the recovery process in other alloys will be crucial for completing the understanding of MG dynamics and clarify the role played by aging on the distribution of anelastic modes. It is important to note, however, that well-controlled conditions and long experimental times are needed to disentangle the pure reversible anelastic effect from

free volume changes and other types of structural evolution that MGs may suffer during the loading and recovery steps. It should also be noted here that our experiments are restricted to small stresses, in the linear regime, and relatively high temperatures $>0.83\,T_g$.

The most accepted microscopic picture of creep deformation of MGs is the presence of localized STZs, with a corresponding distribution of activation energies. For small deformations, the STZs are isolated and are reversible when external stress is released. These isolated STZs would correspond then to the anelastic relaxation modes that originate the large, delayed elasticity phenomenon in MGs. The common interpretation is that the activation of STZs is dependent on their size. The Atzmon model [31,32] proposes a hierarchical distribution of STZs, leading to a distribution of relaxation times characterized by consecutive peaks at discrete times τ_m, with $m = 1, 2, \ldots$, associated to different types of STZs, each one involving different numbers of atoms. The experimental results obtained here could also be interpreted considering a discrete distribution like the one in the Atzmon model. Figures S9(a)–S9(d) in the Supplemental Material [10] show the recovery functions $\phi(t)$ calculated by Eq. (2) using multimodal distributions with a peak intensity $\propto \tau_m^{-0.75}$ (i.e., $\propto \tau_m^{1-0.75}$ in a logarithmic timescale). It can be observed that they cannot be differentiated from the ones originated by a continuous $D(\tau) \propto \tau^{-0.75}$ distribution if the separation between peaks is <1.5 orders of magnitude in time. Another microscopic model is the continuous nucleation of anelastic relaxation sites (or STZs) with a finite lifetime. In such a model, after their lifetime, the anelastic sites relax permanently, thus generating the viscous plastic deformation while they are replaced by the nucleation of new reversible sites. In the steady-state regime, this produces a distribution of anelastic relaxation times of the type $D(\tau) \propto \tau^{-n}$ [9]. It would be interesting to analyze if these and other models can describe all the different features observed here for the recovery functions of Vit4.

Within a more general perspective, the presence of a broad logarithmic or nearly logarithmic relaxation decay is a hallmark of many disordered systems after being subjected to an external excitation [33]. A broad distribution of stress relaxation modes is also observed in athermal systems like granular materials or bead packs, in this case originated by the movement of the particles along stress chains or fields, one particle pushing its neighbors but without hoppinglike, irreversible rearrangements [34]. This is a kind of multiplicative process which produces a broad relaxation time distribution. The broad distribution of modes with a normalized shape not dependent on temperature and the recovery timescale proportional to the excitation time, as found in this paper, indicates that the anelastic deformation and recovery of MGs could be microscopically like this process. This type of atomic drift activated by the previous stress history may explain the compressed exponents and the unexpected short and history-dependent microscopic relaxation times observed by XPCS experiments of MGs [3,39–43]. The long timescales, which are intrinsically associated to temperatures below T_g and well-relaxed glassy states, make the obtention of microscopic insights from molecular dynamics simulations difficult, and a clear microscopic picture that can reproduce all the different experimentally observed features of MG relaxation dynamics is still lacking. We think this paper can afford perspectives and inspire models for elucidating these fundamental issues.

V. CONCLUSIONS

Summarizing, we think that the experimental results and analysis presented here give significant details of the mechanical response of MGs. In this paper, we show that the anelastic relaxation of MGs have a significant amplitude in the region of temperatures spanning from glass transition to 100 K below. Many important mechanical and thermal treatments are applied to MGs in this temperature region [12,44,45], for instance, shape forming and additive manufacture processes as well as heating/cooling protocols to modify the structural state or to release internal stresses. The study of the recovery curves, contrarily to the creep curves, gives access to the pure anelastic response, minimizing the contribution of the viscous component. This reduces the complex effects of aging, offering key information on this subject. The timescale of the anelastic relaxation is found here to be dependent only on the time of previous loading; this fact may be very important to consider to fully understand the results of nanoindentation or other mechanical probes when applied at different rates. All the results presented can be interpreted as the excitation/relaxation of a distribution of reversible deformation modes of the type $D(\tau) \propto \tau^{-n}$, with each mode associated to an activation energy and an exponent n determined by the shape of the loss modulus high-frequency wing. It is worth noting that Vit4 does not show an evident secondary relaxation. In MGs with large secondary relaxations, like Pd-, La-, or Ce-based alloys, a secondary peak will appear in the distribution of anelastic modes. The shape of $\phi(t)$ in such systems would be worth investigating. Although this paper is restricted to Vit4, we think it unveils some important features of the anelastic response which may be general for many disordered systems. This will help the construction of a complete model that can comprehend both reversible and irreversible relaxation processes and explain, in a unified way, the observations in stress step, stress strain, and oscillating strain experiments of MGs, to eventually understand the mechanisms of the atomic mobility.

[1] P. Cao, M. P. Short, and S. Yip, Understanding the mechanisms of amorphous creep through molecular simulation, Proc. Natl. Acad. Sci. U.S.A. **114**, 13631 (2017).

[2] G. B. McKenna, Mechanical rejuvenation in polymer glasses: Fact or fallacy?, J. Phys. Condens. Matter **15**, S737 (2003).

[3] N. Amini, F. Yang, E. Pineda, B. Ruta, M. Sprung, and A. Meyer, Intrinsic relaxation in a supercooled ZrTiNiCuBe glass forming liquid, Phys. Rev. Mater. **5**, 055601 (2021).

[4] L.-M. Wang, R. Liu, and W. H. Wang, Relaxation time dispersions in glass forming metallic liquids and glasses, J. Chem. Phys. **128**, 164503 (2008).

[5] D. Soriano, H. Zhou, S. Hilke, E. Pineda, B. Ruta, and G. Wilde, Relaxation dynamics of Pd-Ni-P metallic glass: Decoupling of anelastic and viscous processes, J. Phys. Condens. Matter **33**, 164004 (2021).

[6] L. C. E. Struik, Physical Aging in Amorphous Polymers and Other Materials, Ph.D. Thesis, Technische Hogeschool Delft, 1977.

[7] Y. J. Lü, C. C. Guo, H. S. Huang, J. A. Gao, H. R. Qin, and W. H. Wang, Quantized aging mode in metallic glass-forming liquids, Acta Mater. **211**, 116873 (2021).

[8] A. I. Taub and F. Spaepen, Ideal elastic, anelastic and viscoelastic deformation of a metallic glass, J. Mater. Sci. **16**, 3087 (1981).

[9] W. Ulfert and H. Kronmüller, Anelastic and viscoelastic behaviour of amorphous $Zr_{65}Cu_{17.5}Ni_{10}Al_{7.5}$ in the range of the glass transition, J. Phys. IV France **06**, C8 (1996).

[10] See Supplemental Material at http://link.aps.org/supplemental/10.1103/PhysRevMaterials.6.125601 for experimental details, additional results, and complementary analyses.

[11] R. Busch, E. Bakke, and W. L. Johnson, Viscosity of the supercooled liquid and relaxation at the glass transition of the $Zr_{46.75}Ti_{8.25}Cu_{7.5}Ni_{10}Be_{27.5}$ bulk metallic glass forming alloy, Acta Mater. **46**, 4725 (1998).

[12] M. A. Gibson, N. M. Mykulowycz, J. Shim, R. Fontana, P. Schmitt, A. Roberts, J. Ketkaew, L. Shao, W. Chen, P. Bordeenithikasem *et al.*, 3D printing metals like thermoplastics: fused filament fabrication of metallic glasses, Mater. Today **21**, 697 (2018).

[13] R. Maddin and T. Masumoto, The deformation of amorphous palladium-20 at. % silicon, Mater. Sci. Eng. **9**, 153 (1972).

[14] Y. Kawamura, T. Nakamura, H. Kato, H. Mano, and A. Inoue, Newtonian and non-Newtonian viscosity of supercooled liquid in metallic glasses, Mater. Sci. Eng. A **304**, 674 (2001).

[15] D. Deng, F. Zheng, Y. Xu, G. Qi, and A. S. Argon, Creep and structural relaxation in Pd40Ni40P20 glass, Acta Metall. Mater. **41**, 1089 (1993).

[16] A. I. Taub and F. E. Luborsky, Creep, stress relaxation and structural change of amorphous alloys, Acta Metall. **29**, 1939 (1981).

[17] V. A. Khonik, A. T. Kosilov, V. A. Mikhailov, and V. V. Sviridov, Isothermal creep of metallic glasses: A new approach and its experimental verification, Acta Mater. **46**, 3399 (1998).

[18] L. Berthier and G. Biroli, Theoretical perspective on the glass transition and amorphous materials, Rev. Mod. Phys. **83**, 587 (2011).

[19] C. Donati, J. F. Douglas, W. Kob, S. J. Plimpton, P. H. Poole, and S. C. Glotzer, Stringlike Cooperative Motion in a Supercooled Liquid, Phys. Rev. Lett. **80**, 2338 (1998).

[20] J. D. Stevenson, J. Schmalian, and P. G. Wolynes, The shapes of cooperatively rearranging regions in glass-forming liquids, Nat. Phys. **2**, 268 (2006).

[21] C. Rainone, E. Bouchbinder, and E. Lerner, Pinching a glass reveals key properties of its soft spots, Proc. Natl. Acad. Sci. U.S.A. **117**, 5228 (2020).

[22] F. Spaepen, a microscopic mechanism for steady state inhomogeneous flow in metallic glasses, Acta Metall. **25**, 407 (1977).

[23] F. Spaepen, Homogeneous flow of metallic glasses: A free volume perspective, Scr. Mater. **54**, 363 (2006).

[24] C. A. Schuh, T. C. Hufnagel, and U. Ramamurty, Mechanical behavior of amorphous alloys, Acta Mater. **55**, 4067 (2007).

[25] M. Bletry, P. Guyot, J. J. Blandin, and J. L. Soubeyroux, Free volume model: High-temperature deformation of a Zr-based bulk metallic glass, Acta Mater. **54**, 1257 (2006).

[26] M. Bletry, P. Guyot, Y. Bréchet, J. J. Blandin, and J. L. Soubeyroux, Transient regimes during high-temperature deformation of a bulk metallic glass: A free volume approach, Acta Mater. **55**, 6331 (2007).

[27] Y. T. Cheng, Q. Hao, J. M. Pelletier, E. Pineda, and J. C. Qiao, Modelling and physical analysis of the high-temperature rheological behavior of a metallic glass, Int. J. Plast. **146**, 103107 (2021).

[28] A. I. Taub and F. Spaepen, Homogeneous flow of amorphous $Pd_{77.5}Cu_6Si_{16.5}$, Scr. Metall. **14**, 1197 (1980).

[29] M. L. Lind, G. Duan, and W. L. Johnson, Isoconfigurational Elastic Constants and Liquid Fragility of a Bulk Metallic Glass Forming Alloy, Phys. Rev. Lett. **97**, 015501 (2006).

[30] A. S. Argon and H. Y. Kuo, Free energy spectra for inelastic deformation of five metallic glass alloys, J. Non. Cryst. Solids **37**, 241 (1980).

[31] J. D. Ju, D. Jang, A. Nwankpa, and M. Atzmon, An atomically quantized hierarchy of shear transformation zones in a metallic glass, J. Appl. Phys. **109**, 053522 (2011).

[32] T. J. Lei, L. R. DaCosta, M. Liu, W. H. Wang, Y. H. Sun, A. L. Greer, and M. Atzmon, Shear transformation zone analysis of anelastic relaxation of a metallic glass reveals distinct properties of α and β relaxations, Phys. Rev. E **100**, 033001 (2019).

[33] A. Amir, Y. Oreg, and Y. Imry, On relaxations and aging of various glasses, Proc. Natl. Acad. Sci. U.S.A. **109**, 1850 (2012).

[34] K. A. Murphy, J. W. Kruppe, and H. M. Jaeger, Memory in Nonmonotonic Stress Relaxation of a Granular System, Phys. Rev. Lett. **124**, 168002 (2020).

[35] S. Havriliak and S. Negami, A complex plane representation of dielectric and mechanical relaxation processes in some polymers, Polymer **8**, 161 (1967).

[36] C. Svanberg, Correlation function for relaxations in disordered materials, J. Appl. Phys. **94**, 4191 (2003).

[37] A. Castellero, B. Moser, D. I. Uhlenhaut, F. H. D. Torre, and J. F. Löffler, Room-temperature creep and structural relaxation of Mg–Cu–Y metallic glasses, Acta Mater. **56**, 3777 (2008).

[38] J. C. Qiao, Q. Wang, J. M. Pelletier, H. Kato, R. Casalini, D. Crespo, E. Pineda, Y. Yao, and Y. Yang, Structural heterogeneities and mechanical behavior of amorphous alloys, Prog. Mater. Sci. **104**, 250 (2019).

[39] B. Ruta, Y. Chushkin, G. Monaco, L. Cipelletti, E. Pineda, P. Bruna, V. M. Giordano, and M. Gonzalez-Silveira,

Atomic-Scale Relaxation Dynamics and Aging in a Metallic Glass Probed by X-Ray Photon Correlation Spectroscopy, Phys. Rev. Lett. **109**, 165701 (2012).

[40] Z. Evenson, B. Ruta, S. Hechler, M. Stolpe, E. Pineda, I. Gallino, and R. Busch, X-Ray Photon Correlation Spectroscopy Reveals Intermittent Aging Dynamics in a Metallic Glass, Phys. Rev. Lett. **115**, 175701 (2015).

[41] V. M. Giordano and B. Ruta, Unveiling the structural arrangements responsible for the atomic dynamics in metallic glasses during physical aging, Nat. Commun. **7**, 10344 (2016).

[42] Z. Evenson, A. Payes-Playa, Y. Chushkin, M. di Michiel, E. Pineda, and B. Ruta, Comparing the atomic and macroscopic aging dynamics in an amorphous and partially crystalline $Zr_{44}Ti_{11}Ni_{10}Cu_{10}Be_{25}$ bulk metallic glass, J. Mater. Res. **32**, 2014 (2017).

[43] B. Ruta, E. Pineda, and Z. Evenson, Relaxation processes and physical aging in metallic glasses, J. Phys. Condens. Matter **29**, 503002 (2017).

[44] G. Kumar, A. Desai, and J. Schroers, Bulk metallic glass: The smaller the better, Adv. Mater. **23**, 461 (2011).

[45] P. He, L. Li, F. Wang, O. Dambon, F. Klocke, K. M. Flores, and A. Y. Yi, Bulk metallic glass mold for high volume fabrication of micro optics, Microsyst. Technol. **22**, 617 (2016).